Innermost stable circular orbit of spinning particle in charged spinning black hole background

Yu-Peng Zhang,* Shao-Wen Wei,† Wen-Di Guo,‡ Tao-Tao Sui,§ and Yu-Xiao Liu‖

Institute of Theoretical Physics, Lanzhou University, Lanzhou 730000, China,
Research Center of Gravitation, Lanzhou University, Lanzhou 730000, China,
and Key Laboratory for Magnetism and Magnetic of the Ministry of Education,
Lanzhou University, Lanzhou 730000, China

(Received 1 December 2017; published 27 April 2018)

In this paper we investigate the innermost stable circular orbit (ISCO) (spin-aligned or anti-aligned orbit) for a classical spinning test particle with the pole-dipole approximation in the background of Kerr-Newman black hole in the equatorial plane. It is shown that the orbit of the spinning particle is related to the spin of the test particle. The motion of the spinning test particle will be superluminal if its spin is too large. We give an additional condition by considering the superluminal constraint for the ISCO in the black hole backgrounds. We obtain numerically the relations between the ISCO and the properties of the black holes and the test particle. It is found that the radius of the ISCO for a spinning test particle is smaller than that of a nonspinning test particle in the black hole backgrounds.

DOI: 10.1103/PhysRevD.97.084056

I. INTRODUCTION

In the Newtonian gravitational theory we know that a massive particle can orbit around a central celestial body in the gravitational field generated by the central celestial body. Coincidentally, in general relativity a massless or massive particle can also orbit around a central celestial body and the properties of the central celestial body will affect the motion of the particle orbiting it. In Ref. [1] Kaplan first investigated a nonspinning massive test particle orbiting a Schwarzschild black hole and found that there exists a stable circular orbit with a minimal radius $3r_h$, where the r_h is the radius of the horizon of the Schwarzschild black hole. This orbit is the innermost stable circular orbit (ISCO) [2].

It is well known that the gravitational waves have been detected directly by LIGO and VIRGO [3–7] and the binary black hole/neutron star systems are the most important sources of gravitational waves. When the mass ratio of the binary systems is extreme, a binary system can be approximated as a test body spiraling into a supermassive black hole in galaxy, which is one of the most important sources of gravitational waves and might be detected by the future space-based detectors: Laser Interferometer Space Antenna (LISA) [8], Taiji, and Tianqin [9]. Note that the circular (timelike) orbits locate inner the ISCO are unstable under perturbations away from circularity, and the ISCO can be treated as the start of final merger of the binary system. The ISCO of a black hole can also give the properties about the spacetime geometry of the black hole background, since the motion of the test particle depends on both the spin and charge of the black hole. The ISCOs in different black hole backgrounds were investigated systematically in Refs. [10–35].

We know that the motion of a test particle should be geodesic. When the reaction of the test particle is considered, the corresponding motion will not be geodesic any more [28,36,37]. In addition to the geodesic deviation resulted by the reaction of the test particle, the spin of the test particle can also lead to the motion of the test particle is not geodesic due to an additional force (spin-curvature force) resulted from the spin [38,39]. In this paper we only consider the spin of the test particle and neglect the reaction to the background and investigate the ISCO of the spinning test particle in black hole backgrounds. The ISCO of a spinning test particle in the Schwarzschild and Kerr spacetimes was firstly investigated numerically in Ref. [10]. In Ref. [40], Jefremov, Tsupko, and Bisnovatyi-Kogan numerically investigated the ISCO of the spinning test particle in the Schwarzschild and Kerr spacetimes and gave the approximate analytic solutions of the ISCO for the particle with a small spin.

The equations of motion for a spinning particle in curved spacetime were obtained in the "pole-dipole" approximation in Refs. [41–48]. For the motion of a spinning test particle in curved spacetime, the corresponding velocity

*zhangyupeng14@lzu.edu.cn
†weishw@lzu.edu.cn
‡guowd14@lzu.edu.cn
§suitt14@lzu.edu.cn
‖Corresponding author.
liuyx@lzu.edu.cn

 © 2018 American Physical Society

vector u^μ and the canonical momentum vector P^μ are not parallel [45,49,50]. The canonical momentum vector P^μ keeps timelike along the trajectory and satisfies $P^\mu P_\mu = -m^2$ (where the parameter m is the mass of the test particle) while the velocity vector u^μ might transform to be spacelike from timelike [45,49,50] if the spin of the test particle is too large. Note that the "pole-dipole" approximation will be a serious problem in highly nonhomogeneous fields due to the neglect of the multipole effect. In Refs. [51–54] the authors suggested a way to avoid the superluminal problem by considering the multipole effect of the spinning test particle by introducing a nonminimal interaction of spin with gravity through gravimagnetic moment. For the description of self-gravitating compact objects and the gravitational radiation emitted by the compact objects, the effects of multipole for the spinning test particle should be considered [55]. The chaos and the gravitational radiation of the spinning test particle were investigated in Refs. [56–58].

In this paper we only consider the "pole-dipole" approximation for simplicity and investigate the ISCO of a spinning test particle with arbitrary spin s in black hole background with the superluminal constraint. We numerically give the ISCO parameters of the spinning test particle in Kerr-Newman (KN) black hole background with the Tulczyjew spin-supplementary condition. We find that the radius of the ISCO for a spinning test particle is smaller than that of a nonspinning test particle in KN black hole background, which is consistent with the results obtained in Refs. [10,40]. We also investigate how the ISCO of a spinning test particle is affected by the properties of the black hole and the spin of the test particle with the additional superluminal constraint.

Our paper is organized as follows. In Sec. II we review the equations of motion for a spinning test particle in curved spacetime and obtain the corresponding four-momentum and four-velocity in KN black hole background. In Sec. III we give a new condition for solving the ISCO of the spinning test particle with superluminal constraint in black hole background, and we also investigate how the characters of the ISCO for the spinning test particle are affected by the particle's spin s and the black hole charge and spin. Finally, a brief summary and conclusion are given in Sec. IV.

II. MOTION OF A SPINNING TEST PARTICLE IN KERR-NEWMAN BLACK HOLE BACKGROUND

In this section, we review the equations of motion of a spinning test particle in curved spacetime. The effect of the spin of a test particle on its motion was first derived by considering that the test particle's spin is coupled with curvature [42,43], and the equations of motion can be derived with several methods [41,44,45,50,59]. Here, we use the Lagrangian to derive the equations of motion for a spinning test particle based on Refs. [45,50]. The position and orientation of a spinning test particle can be represented by the coordinate x^μ and the orthonormal tetrad $e^\mu_{(\alpha)}$, respectively. The tetrad $e^\mu_{(\alpha)}$ satisfies the relation $g^{\mu\nu} = e^\mu_{(\alpha)} e^\nu_{(\beta)} \eta^{(\alpha\beta)}$. We define the four-velocity of the spinning test particle as follows

$$u^\mu \equiv \frac{dx^\mu}{d\lambda}, \tag{1}$$

where λ is the affine parameter. For the spinning test particle the corresponding angular velocity tensor $\sigma^{\mu\nu}$ is defined as

$$\sigma^{\mu\nu} \equiv \eta^{(\alpha\beta)} e^\mu_{(\alpha)} \frac{De^\nu_{(\beta)}}{D\lambda} = -\sigma^{\nu\mu}, \tag{2}$$

where $\frac{De^\nu_{(\beta)}}{D\lambda}$ is the covariant derivative of the tetrad and has the form

$$\frac{De^\nu_{(\beta)}}{D\lambda} \equiv \frac{de^\nu_{(\beta)}}{d\lambda} + \Gamma^\nu_{\rho\tau} e^\rho_{(\beta)} u^\tau. \tag{3}$$

The Lagrangian $\mathcal{L}$ that describes the spinning test particle in curved spacetime can be constructed in terms of invariant quantities. There are four independent invariants [45,46]:

$$\begin{aligned} a_1 &= u^\mu u_\mu, \\ a_2 &= \sigma^{\mu\nu}\sigma_{\mu\nu} = -\mathrm{tr}(\sigma^2), \\ a_3 &= u_\alpha \sigma^{\alpha\beta}\sigma_{\beta\gamma} u^\gamma, \\ a_4 &= g_{\mu\nu} g_{\rho\tau} g_{\alpha\beta} g_{\gamma\delta} \sigma^{\delta\mu}\sigma^{\nu\rho}\sigma^{\tau\alpha}\sigma^{\beta\gamma}. \end{aligned} \tag{4}$$

Then the final equations of motion for the spinning particle can be derived by using $\mathcal{L} = \mathcal{L}(a_1, a_2, a_3, a_4)$ [45] with the "pole-dipole" approximation as follows

$$\frac{DP^\mu}{D\lambda} = -\frac{1}{2} R^\mu_{\nu\alpha\beta} u^\nu S^{\alpha\beta}, \tag{5}$$

$$\frac{DS^{\mu\nu}}{D\lambda} = S^{\mu\lambda}\sigma^\nu_\lambda - \sigma^{\mu\lambda} S^\nu_\lambda = P^\mu u^\nu - u^\mu P^\nu. \tag{6}$$

Obviously, the motion of a spinning test particle does not follow the geodesic due to the spin-curvature force $-\frac{1}{2} R^\mu_{\nu\alpha\beta} u^\nu S^{\alpha\beta}$.

Note that the choice of the spin-supplementary condition is related to the center of mass of the a spinning test particle with different observers, so the choice of the spin-supplementary condition is not unique [60]. And the worldlines of the test particles with different spin-supplementary conditions are not same, for example, the worldline of the spinning test particle is a circular motion or helical motion superposed on the averaged circular

motion with different spin-supplementary conditions [61]. That is to say the different spin-supplementary condition will give a different radius for the ISCO [62]. In this paper we only choose the Tulczyjew spin-supplementary condition

$$P_\mu S^{\mu\nu} = 0, \tag{7}$$

where P_μ and $S_{\mu\nu}$ are the conjugate momentum vector and spin tensor, respectively, and they are defined by

$$P_\mu \equiv \frac{\partial \mathcal{L}}{\partial u^\mu}, \qquad S_{\mu\nu} \equiv \frac{\partial \mathcal{L}}{\partial \sigma^{\mu\nu}} = -S_{\nu\mu}. \tag{8}$$

Here, we should note that for the spinning test particle the canonical momentum P^μ satisfies $P^\mu P_\mu = -m^2$, which means that the canonical momentum P^μ keeps timelike along the trajectory. However, things will be different for the velocity vector u^μ, which may transform from timelike to spacelike as it is not parallel to P^μ [45,49,50].

Next we will solve the equations of motion of the spinning test particle in the KN black hole background. The KN black hole background can be described by the Boyer-Lindquist coordinates

$$ds^2 = -\frac{\Delta}{\rho^2}(dt - a\sin^2\theta d\phi)^2 + \frac{\rho^2}{\Delta}dr^2 + \rho^2 d\theta^2 + \frac{\sin^2\theta}{\rho^2}[(r^2+a^2)d\phi - a dt]^2, \tag{9}$$

where the metric functions Δ and ρ^2 are

$$\Delta = r^2 - 2Mr + a^2 + Q^2, \qquad \rho^2 = r^2 + a^2\cos^2\theta. \tag{10}$$

Here Q, M, and a are the charge, mass, and spin of the black hole, respectively. The KN black hole has outer and inner horizons $r_\pm = 1 \pm \sqrt{1-(a^2+Q^2)}$ and we have chosen $M = 1$ for simplicity. The charge and spin of the KN black hole should satisfy the constraint

$$a^2 + Q^2 \le 1, \tag{11}$$

where "=" corresponds to the extremal black hole with one degenerate horizon.

In this paper, we only consider the equatorial motion of the test particle with $\theta = \frac{\pi}{2}$. So the nonvanishing components of the conjugate momentum are [46,63]

$$P^t = \frac{m^3}{\Theta\Xi}[r^2 a\bar{j}(2Mr - Q^2) - \bar{e}r^6 + (2a\bar{e} - \bar{j})Q^2 r^2 \bar{s} - r^2 a^2 \bar{e}(2Mr + r^2 - Q^2) + (\bar{j} - 3a\bar{e})Mr^3\bar{s} + a^2(a\bar{e} - \bar{j})(Q^2 - Mr)\bar{s}], \tag{12}$$

$$P^\phi = \frac{m^3}{\Theta\Xi}[a\bar{e}r^2(Q^2 - 2Mr) + a^2\bar{e}(Q^2 - Mr)\bar{s} + r^2 Q^2 + a\bar{j}(Mr - Q^2)\bar{s} + r^2(r^2 - 2Mr)(\bar{e}\,\bar{s} - \bar{j})], \tag{13}$$

and

$$(P^r)^2 = \frac{m^6}{r^2\Xi^2}[r^6(2Mr^3 - r^2(\bar{j}^2 + a^2 - a^2\bar{e}^2 + Q^2) + j_e^2(2Mr - Q^2) + (\bar{e}^2 - 1)r^4) - 2r^4\bar{s}(aQ_r j_e^2 - 2\bar{e}j_e Q^2 r^2 + 3\bar{e}j_e Mr^3 - \bar{e}\,\bar{j}\,r^4) - Q_r^2\Theta\bar{s}^4 + r^2\bar{s}^2 a^2 Q_r\bar{e}^2(Q_r + 2r^2) + r^2\bar{s}^2(\bar{j}^2 Q_r^2 - 2a\bar{e}\,\bar{j}\,Q_r(Q_r + r^2) - a^2 Q_r 2r^2 - r^2(Q^2 + r^2 - 2Mr)(\bar{e}^2 r^2 + 2Q_r))]. \tag{14}$$

Here the parameters $\bar{e} \equiv \frac{e}{m}$, $\bar{s} \equiv \frac{s}{m}$, and $\bar{j} \equiv \frac{j}{m} = \frac{l}{m} + \frac{s}{m}$ are the energy, spin angular momentum, and total angular momentum per unit mass of the test particle, respectively. The parameter l is the orbital angular momentum of the test particle and Θ, Ξ, and Q_r are defined as [63]

$$\Theta \equiv a^2 + Q^2 - 2Mr + r^2, \tag{15}$$

$$\Xi \equiv m^2 r^4 + (Q^2 - Mr)m^2\bar{s}^2, \tag{16}$$

$$Q_r \equiv Q^2 - Mr, \qquad j_e \equiv \bar{j} - a\bar{e}. \tag{17}$$

The velocity u^μ can be solved according to the equations of motion (5) and (6) [50]

$$\frac{DS^{tr}}{D\lambda} = P^t\dot{r} - P^r \tag{18}$$

$$\frac{DS^{t\phi}}{D\lambda} = P^t\dot{\phi} - P^\phi. \tag{19}$$

For simplicity, we only consider the spin-aligned or antialigned orbits. The nonvanishing components of the spin tensor $S^{\mu\nu}$ in the KN black hole background are

$$S^{r\phi} = -S^{\phi r} = -\frac{sP_t}{mr}, \quad S^{rt} = -S^{tr} = -S^{r\phi}\frac{P_\phi}{P_t} = s\frac{P_\phi}{mr}, \quad S^{\phi t} = -S^{t\phi} = S^{r\phi}\frac{P_r}{P_t} = -s\frac{P_r}{mr}. \tag{20}$$

Equations (18) and (19) can be expressed in terms of Eq. (26) as follows

$$\frac{DS^{tr}}{D\lambda} = P^t\dot{r} - P^r = \frac{1}{2}\frac{s}{mr}g_{\phi\mu}R^\mu_{\nu\alpha\beta}u^\nu S^{\alpha\beta} + s\frac{P_\phi}{mr^2}\dot{r} \tag{21}$$

and

$$\frac{DS^{t\phi}}{D\lambda} = P^t\dot{\phi} - P^\phi = -\frac{1}{2}\frac{s}{mr}g_{r\mu}R^\mu_{\nu\alpha\beta}u^\nu S^{\alpha\beta} - s\frac{P_r}{mr^2}\dot{r}. \tag{22}$$

Substituting the nonvanishing components of the Riemman curvature tensor of the KN black hole background into Eqs. (21) and (22), the nonzero components of the four-velocity are [63]

$$\begin{aligned}\dot{r} = P^r\Delta[&m^2r^6 + r^2(q^2-r)s^2][m^2P^tr^6\Delta \\ &+ [(-P_\phi + aP_t)q^2(4a^3+3aq^2) - msP_\phi r^4\Delta \\ &+ a(3P_\phi - 4aP_t)r^3 + a(P_\phi - aP_t)(3a^2+8q^2)r \\ &+ a[-4P_\phi(1+q^2) + aP_t(4+5q^2)]r^2 \\ &+ P_tq^2r^4 - P_tr^5]s^2]^{-1}\end{aligned} \tag{23}$$

and

$$\begin{aligned}\dot{\phi} = K_2^{-1}\Big\{&a^3P_ts^2(4q^2-3r) + [a^2+q^2+r(r-2)] \\ &\times\left[\frac{K_1}{K_2} + m^2P^\phi r^6 + P_\phi s^2(3r-4q^2)\right] \\ &+ a^2[P_\phi s^2(3r-4q^2)] + [q^2+r(r-2)] \\ &\times[P_\phi s^2(2r-3q^2)] \\ &+ aP_ts^2[3q^4 + 4q^2(r-2)r + r^2(4-3r)]\Big\},\end{aligned} \tag{24}$$

where $v^r = \dot{r}$, $v^\phi = \dot{\phi}$, and K_i $(i = 1, 2)$ is defined as follows

$$K_1 = -mP_rr^4s\Delta[P_rs^2(q^2-r)\Delta + m^2P^rr^6], \tag{25}$$

$$\begin{aligned}K_2 = &m^2P^tr^6\Delta - mP_\phi r^4s\Delta \\ &+ s^2[q^2(4a^3+3aq^2)(aP_t - P_\phi) \\ &+ ar(3a^2+8q^2)(P_\phi - aP_t) \\ &+ ar^2(aP_t(5q^2+4) - 4P_\phi(q^2+1)) \\ &+ ar^3(3P_\phi - 4aP_t) + P_tq^2r^4 - P_tr^5].\end{aligned} \tag{26}$$

The orbital frequency parameter Ω is defined as

$$\Omega = \dot{\phi}. \tag{27}$$

Obviously, it can be seen from Eq. (23) that the radial momentum P^r and radial velocity v^r are parallel. So we can use the radial component P^r of the four-momentum to define the effective potential for the spinning test particle.

III. ISCO OF A SPINNING PARTICLE IN KERR-NEWMAN BLACK HOLE BACKGROUND

In this section, we will investigate the ISCO of the spinning test particle in different black hole backgrounds. As stated in the previous paper and book [1,64], the motion of a test particle in a central field can be solved in terms of the radial coordinate "effective potential" in the Newtonian dynamics. And the so-called "effective potential" method is also generalized to general relativity to solve the motion of a test particle in black hole backgrounds. We know that if a test particle satisfies the following two conditions [40]:

(a) the radial velocity of the test particle vanishes:

$$\frac{dr}{d\lambda} = 0. \tag{28}$$

(b) the radial velocity should keep unchanged, which means that the acceleration of the radial velocity should be zero:

$$\frac{d^2r}{d\lambda^2} = 0. \tag{29}$$

Then the corresponding trajectory of the test particle must be a stable circular orbit. As stated in Ref. [40], we know that there is an ISCO when radius of the stable circular orbit is minimal. So the ISCO locates at the point that the maximum and minimum of the effective potential merge. It is obvious that for the ISCO the effective potential of the test particle should also satisfy

$$\frac{d^2V_{\text{eff}}}{dr^2} = 0. \tag{30}$$

So we can use these three conditions (28), (29), and (30) to get the ISCO of the test particle.

For the Schwarzschild black hole, the corresponding effective potential of a nonspinning test particle is

$$V_{\text{eff}}^{\text{Schw}} = \sqrt{\left(1-\frac{2M}{r}\right)\left(1+\frac{\bar{l}^2}{r^2}\right)}, \tag{31}$$

and the parameters of the ISCO of the test particle are [1]

$$r_{\text{ISCO}} = 6M, \quad \bar{l}_{\text{ISCO}} = 2\sqrt{3}M, \quad \bar{e}_{\text{ISCO}} = \sqrt{\frac{8}{9}}, \tag{32}$$

where the parameters $\bar{l}$ and $\bar{e}$ are the orbital angular momentum and energy per unit rest mass of the test particle, respectively. If the test particle moves along a circular orbit, its energy should be the minimum value of the effective potential. For example, the corresponding orbits of the nonspinning test particle with different energies are shown in Fig. 1.

For the Kerr black hole, the ISCO was given in Ref. [65] for the extremal case with $a = M$. Due to the drag effect of the Kerr black hole, the ISCOs with counterrotating orbit and corotating orbit are different and the corresponding results are respectively

$$r_{\text{ISCO}} = 9M, \quad \bar{l}_{\text{ISCO}} = -\frac{22}{3\sqrt{3}}M, \quad \bar{e}_{\text{ISCO}} = \frac{5}{3\sqrt{3}}, \tag{33}$$

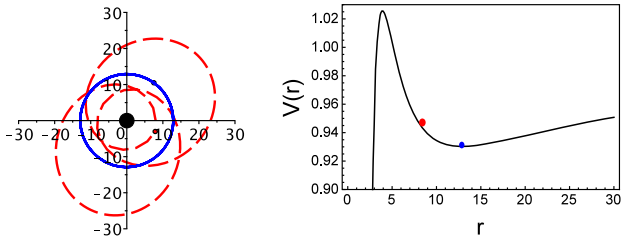

FIG. 1. Plots of the orbits and effective potential for the nonspinning test particle in the Schwarzschild black hole background. The blue dot means the particle locates at the minimum value of the effective potential and the corresponding orbit is circular orbit (blue solid line), while the red dot stands for the test particle with energy $\bar{e} \approx 0.9461$ and orbital angular momentum $\bar{l} = 4.1$ and the corresponding orbit (red dashed line) is not a circular orbit.

and

$$r_{\rm ISCO} = M, \quad \bar{l}_{\rm ISCO} = \frac{2}{\sqrt{3}}M, \quad \bar{e}_{\rm ISCO} = \frac{1}{\sqrt{3}}. \quad (34)$$

Next, we will investigate the ISCO of the spinning test particle in the KN black hole background. In Sec. II we have solved the four-momentum and velocity of the spinning test particle by using the equations of motion (5) and (6). Since the radial velocity and radial component P^r of the four-momentum are parallel, we can use P^r to define the effective potential of the spinning test particle in black hole background. The square of P^r reads

$$\begin{aligned}(P^r)^2 = \frac{m^6}{r^2\Xi^2}[&r^6(2Mr^3 - r^2(\bar{j}^2 + a^2 - a^2\bar{e}^2 + Q^2) \\ &+ j_e^2(2Mr - Q^2) + (\bar{e}^2 - 1)r^4) \\ &- 2r^4\bar{s}(aQ_r j_e^2 - 2\bar{e}j_e Q^2 r^2 + 3\bar{e}j_e Mr^3 - \bar{e}\,\bar{j}\,r^4) \\ &- Q_r^2\Theta\bar{s}^4 + r^2\bar{s}^2a^2Q_r\bar{e}^2(Q_r + 2r^2) \\ &+ r^2\bar{s}^2(\bar{j}^2Q_r^2 - 2a\bar{e}\,\bar{j}\,Q_r(Q_r + r^2) - a^2Q_r 2r^2 \\ &- r^2(Q^2 + r^2 - 2Mr)(\bar{e}^2r^2 + 2Q_r))], \end{aligned} \quad (35)$$

which can be decomposed as follows

$$\begin{aligned}(P^r)^2 &= \frac{m^6}{r^2\Xi^2}(\alpha e^2 + \beta e + \gamma) \\ &= \frac{m^6}{r^2\Xi^2}\left(e - \frac{-\beta + \sqrt{\beta^2 - 4\alpha\gamma}}{2\alpha}\right) \\ &\quad \times \left(e + \frac{\beta + \sqrt{\beta^2 - 4\alpha\gamma}}{2\alpha}\right), \end{aligned} \quad (36)$$

where the functions α, β, and γ are

$$\begin{aligned}\alpha = &m^2r^6(a^2(2Mr + r^2 - Q^2) + r^4) \\ &+ 2amr^4s(a^2(Mr - Q^2) + r^2(3Mr - 2Q^2)) \\ &+ r^2s^2[a^2(Q^2 - Mr)(Q^2 - r(M + 2r)) \\ &- r^4(r(r - 2M) + Q^2)], \end{aligned} \quad (37)$$

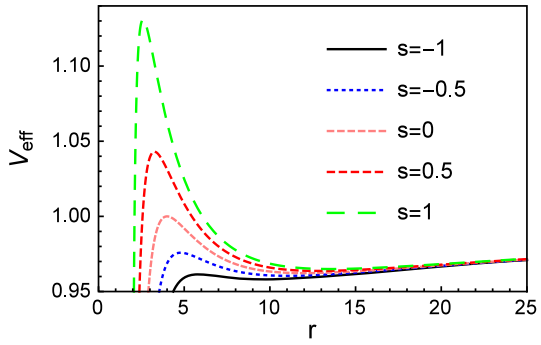

FIG. 2. Plots of the effective potential (40) for the spinning test particle with different spins, the parameters are set as $a = 0$, $Q = 0$, and $l = 4$.

$$\begin{aligned}\beta = &2jr^2[2a^2mr^2s(Q^2 - Mr) + am^2r^4(Q^2 - 2Mr) \\ &- as^2(Q^2 - Mr)(Q^2 - r(M + r)) \\ &+ mr^4s(r(r - 3M) + 2Q^2)], \end{aligned} \quad (38)$$

and

$$\begin{aligned}\gamma = &j^2r^2[2amr^2s(Mr - Q^2) \\ &- m^2r^4(-2Mr + Q^2 + r^2) + s^2(Q^2 - Mr)^2] \\ &- \Delta(s^2(Q^2 - Mr) + m^2r^4)^2. \end{aligned} \quad (39)$$

The effective potential of the spinning test particle in the KN black hole background is

$$V_{\rm eff}^{\rm spin} = \frac{-\beta + \sqrt{\beta^2 - 4\alpha\gamma}}{2\alpha}. \quad (40)$$

For the case of $s = 0$, our result (40) can reduce to that of the KN black hole. Plots of the effective $V_{\rm eff}^{\rm spin}$ with different spins are shown in Fig. 2.

Note that the effective potential of the spinning test particle is dependent on the spin of the test particle. We know that there are two extreme points in the effective potential. The orbits of the test particle corresponding to the two extreme points are circular, and one is unstable while the other is stable. We give the relation of the circular orbit radius r and the orbital angular momentum l with different values of the spin s in Fig. 3. The point that the upper and lower curves intersect defines the ISCO of the spinning test particle. It is evident that the radius of the ISCO decreases (increases) with the spin s when the direction of the angular momentum of the test is the same as (the opposite of) that of the black hole.

We can solve the ISCO of the spinning test particle in terms of the three conditions (28), (29), and (30). Here we note that the four-velocity and four-momentum are not parallel [45,49,50,63] and the velocity may transform from timelike to spacelike, which means that the ISCO of the spinning test particle may be unphysical. So we should add the superluminal constraint

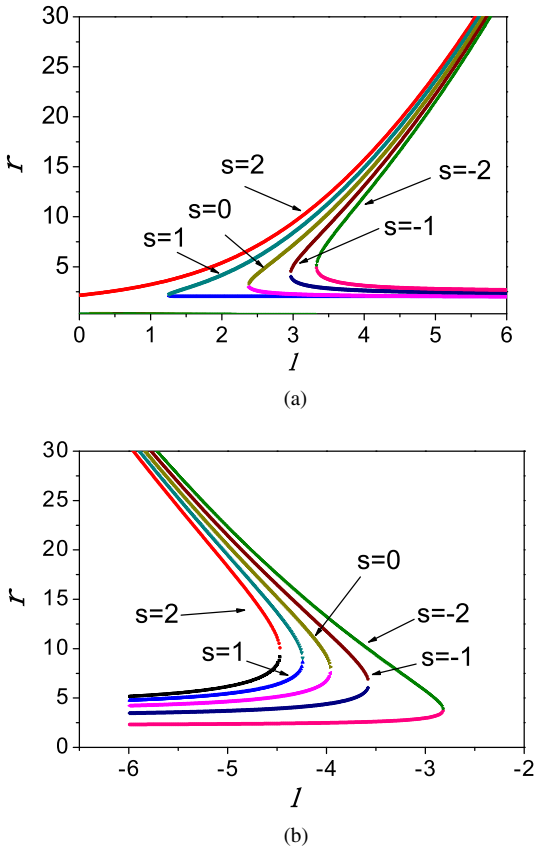

FIG. 3. The relation between circular orbit radius r and orbital angular momentum l for different values of the spin s, where the upper curves stand for the stable circular orbits while the lower curves stand for the unstable circular orbits. Here the subfigure (a) describes the corotating orbits and subfigure (b) describes counterrotating orbits. The parameters are set as $a = 0.5$, $Q = 0.5$.

$$\frac{u^\mu u_\mu}{(u^t)^2} = \frac{g_{tt}}{c^2} + g_{rr}\left(\frac{\dot{r}}{c}\right)^2 + g_{\phi\phi}\left(\frac{\dot{\phi}}{c}\right)^2 + 2g_{\phi t}\dot{\phi} < 0, \tag{41}$$

which ensures that the motion of the spinning test particle in circular orbit is subluminal. In Refs. [40], the authors obtained the analytical corrections to the ISCO for the spinning test particle with small-spin linear approach for the Schwarzschild and Kerr black holes, and numerically investigated the effect of the spin on the ISCO without the superluminal constraint (41).

In summary, if we want to solve the physical ISCO of the spinning test particle, we should use the four conditions (28), (29), (30), and (41). First, we numerically give the region that whether the spinning test particle has a timelike circular orbit in the $(s - l)$ parameter space. For simplicity, we only give the result for the Schwarzschild black hole in Fig. 4. Obviously, some circular orbits in the parameter space are spacelike and unphysical. So it is necessary to consider the constraint (41) for the ISCO of the spinning test particle.

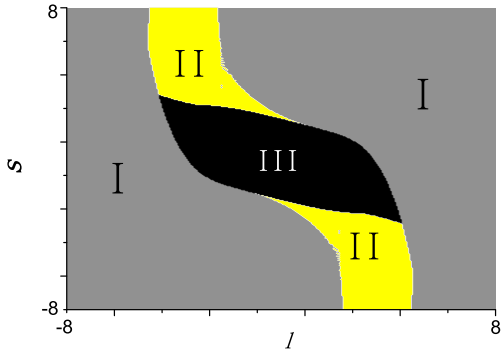

FIG. 4. Plot of the region that the spinning test particle has a circular orbit in the $(s - l)$ parameter space. Region II (yellow region) stands for that the motion of the spinning test particle in the circular orbit is superluminal and unphysical, region III (black region) stands for that the spinning test particle does not have a circular orbit, region I (gray region) stands for that the spinning test particle can have a physical circular orbit.

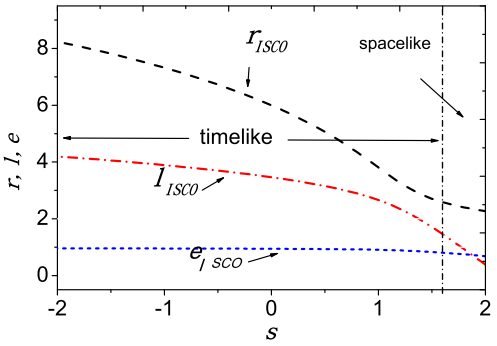

FIG. 5. Plot of the ISCO parameters of the spinning test particle as functions of the spin s in the Schwarzschild black hole background. The left side of the vertical line stands for that the ISCO is timelike and physical, while the right side stands for that the orbit is spacelike and unphysical.

To proceed, we numerically investigate the effects of the spin of the test particle on the ISCO in different black hole backgrounds with the superluminal constraint (41) in detail. First, we give the complete numerical results for the ISCO of the spinning test particle in the Schwarzschild black hole background. The corresponding numerical results are shown in Fig. 5. It can be seen that the ISCO parameters of the spinning test particle will decrease with the spin s. The physical ISCO parameters of the spinning test particle in the Schwarzschild black hole background with the superluminal bound are calculated as follows

$$\begin{aligned} \bar{s}^{\mathrm{Sch}}_{\mathrm{ISCO}} &\approx 1.6510M, & r^{\mathrm{Sch}}_{\mathrm{ISCO}} &\approx 2.5308M, \\ \bar{e}^{\mathrm{Sch}}_{\mathrm{ISCO}} &\approx 0.7896, & \bar{l}^{\mathrm{Sch}}_{\mathrm{ISCO}} &\approx 1.3249M. \end{aligned} \tag{42}$$

We find that the radius of the ISCO for the spinning test particle is smaller than that of the nonspinning test particle in the Schwarzschild black hole background.

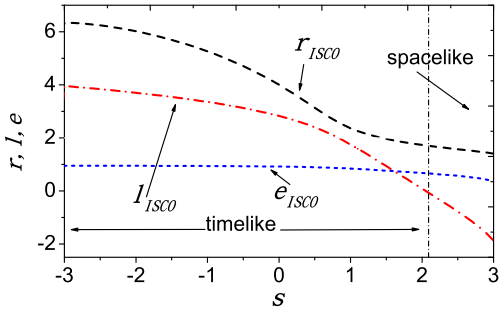

FIG. 6. Plots of the ISCO parameters of the spinning test particle as functions of the spin s in the RN black hole background. The left side of the vertical line stands for that the orbit of the ISCO is timelike and physical, while the right side stands for that the orbit is spacelike and unphysical. The parameters are set as $a/M = 0$, $Q/M = 1$.

We know that the RN black hole is charged and its charge Q will affect the effective potential (40) of the test particle. The numerical results of the ISCO with different values of the charge Q and spin s are given in Fig. 6. For the charged black hole, we can see that the radius of the ISCO of the spinning test particle also decreases with the spin s, and some orbits are also superluminal. Note that the radius of the ISCO for the spinning test particle also decreases with the charge Q, which is consistent with the results in Ref. [34]. The corresponding physical ISCO parameters of the spinning test particle in the extremal RN black hole background with the superluminal bound are

$$\bar{s}^{\mathrm{RN}}_{\mathrm{ISCO}} \approx 2.1490M, \qquad r^{\mathrm{RN}}_{\mathrm{ISCO}} \approx 1.6833M,$$
$$\bar{e}^{\mathrm{RN}}_{\mathrm{ISCO}} \approx 0.6474, \qquad \bar{l}^{\mathrm{RN}}_{\mathrm{ISCO}} \approx -0.1658M. \tag{43}$$

Obviously, the radius of the ISCO of the spinning test particle in the charged black hole background is smaller than that in the background of the Schwarzschild black hole with the same mass M. The radius of the ISCO for the spinning test particle with different values of the black hole charge Q and s are shown in Fig. 7.

It is easy to know that the motion of a spinning test particle also depends on the spin of the black hole. The ISCO of the spinning test particle with corotating orbit in the Kerr black hole background has the same behavior with the spin s changing in the Schwarzschild and RN black hole cases, and the radius of the ISCO also decreases with the black hole spin a. The radius of the ISCO for the spinning test particle with different values of the spin a and s are shown in Fig. 8 and our numerical results are the same as in Ref. [40]. It should be noted that the limiting values of the radius and frequency of the ISCO parameters for the spinning test particle for $a = M$ do not depend on the particles's spin. The corresponding numerical results of the ISCO with co-rotating orbits and counter-rotating orbits in the Kerr black hole background are shown in Fig. 9.

The corresponding ISCO parameters for the counter-rotating or corotating orbits of the nonspinning test particle

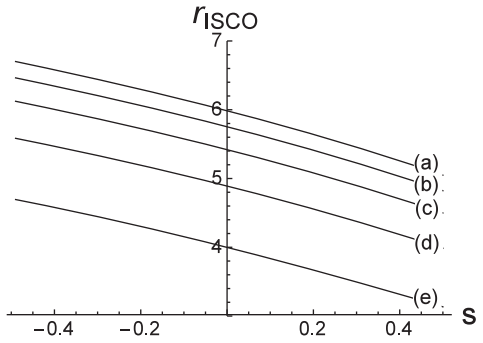

FIG. 7. Plots of the radius of the ISCO of the spinning test particle as functions of the spin s in the RN black hole background, the values of Q approach to M and set as $Q/M = 0.2$ (a), $Q/M = 0.4$ (b), $Q/M = 0.6$ (c), $Q/M = 0.8$ (d), $Q/M = 1$ (e).

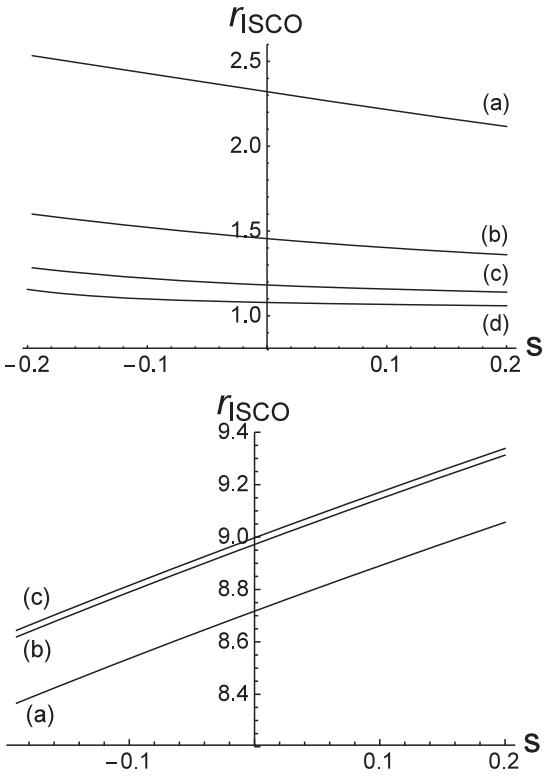

FIG. 8. Plots of the radius of the ISCO of the spinning test particle with corotating and counterrotating orbit as functions of the spin s in the Kerr black hole background, the values of a approach to M and set as $a/M = 0.9$ (a), $a/M = 0.99$ (b), $a/M = 0.999$ (c), $a/M = 0.9999$ (d).

in the extremal Kerr black hole background are given in Eqs. (33) and (34). Note that the radius of the ISCO with co-rotating orbit is

$$r_{\mathrm{ISCO}} = M = r_h. \tag{44}$$

Obviously, the ISCO of the spinning test particle in extremal Kerr black hole background is interesting and needed to investigate in detail. In Ref. [40], the authors

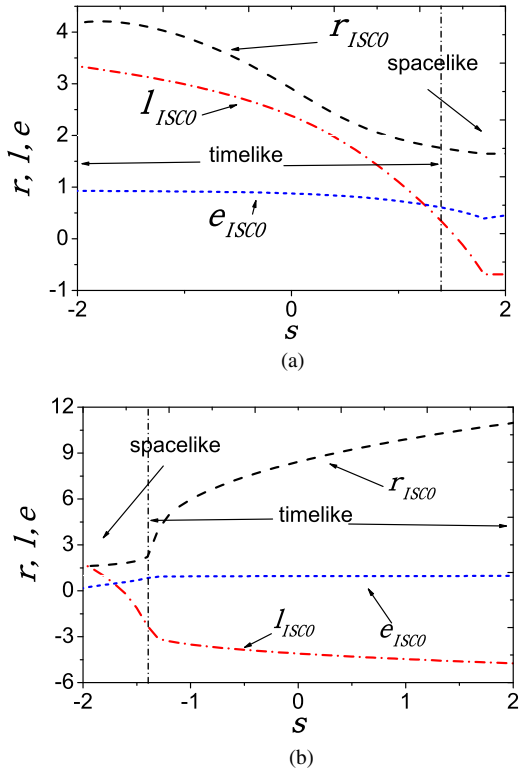

FIG. 9. Plots of the ISCO parameters of the spinning test particle with (a) corotating orbit and (b) counterrotating orbit as functions of the spin s in the Kerr black hole background. Only the left (right) side of the vertical line in upper (lower) figure stands for the timelike orbit. The parameters are set as $a/M = 0.8$, $Q/M = 0$

investigated the behavior of the ISCO for the spinning test particle in the limit of $a = M$ and showed that the limiting values of the ISCO radius and frequency is independent of the spin of test particle while the values of the energy and total angular momentum do depend on it in the small spin s approximation. By comparing our results in Tables I and II and the results in Ref. [40], we find that our results have the

TABLE I. The ISCO parameters of the spinning test particle with corotating orbits in KN black hole background with charge $Q/M = 0$ and spin $a/M = 0.99999$.

s	r_{ISCO}	l_{ISCO}	e_{ISCO}	$\Omega^2_{\bar{s}}$
−0.1000	1.0456	1.4067	0.6529	0.6167
−0.0800	1.0426	1.3634	0.6412	0.6173
−0.0600	1.0403	1.3205	0.6298	0.6179
−0.0400	1.0383	1.2781	0.6186	0.6183
−0.0200	1.0367	1.2361	0.6075	0.6187
0.0000	1.0352	1.1944	0.5967	0.6190
0.0200	1.0340	1.1530	0.5860	0.6193
0.0400	1.0328	1.1118	0.5754	0.6196
0.0600	1.0318	1.0709	0.5649	0.6198
0.0800	1.0308	1.0301	0.5545	0.6201
0.1000	1.0300	0.9895	0.5442	0.6203

TABLE II. The ISCO parameters of the spinning test particle with corotating orbits in KN black hole background with charge $Q/M = 0$ and spin $a/M = 0.999999$.

s	r_{ISCO}	l_{ISCO}	e_{ISCO}	$\Omega^2_{\bar{s}}$
−0.1000	1.0211	1.3912	0.6455	0.6238
−0.0800	1.0196	1.3463	0.6331	0.6241
−0.0600	1.0185	1.3022	0.6210	0.6244
−0.0400	1.0176	1.2587	0.6092	0.6246
−0.0200	1.0168	1.2156	0.5977	0.6248
0.0000	1.0161	1.1731	0.5864	0.6249
0.0200	1.0155	1.1309	0.5753	0.6251
0.0400	1.0150	1.0890	0.5644	0.6252
0.0600	1.0145	1.0474	0.5536	0.6253
0.0800	1.0141	1.0060	0.5429	0.6254
0.1000	1.0137	0.9648	0.5323	0.6255

same behavior for the ISCO of the spinning test particle with small spin s in the quasiextremal kerr black hole background.

For the ISCO with counterrotating orbit the corresponding radius can be smaller due to the existence of the spin s. The physical ISCO parameters of the spinning test particle with counterrotating orbit in the extremal Kerr black hole background with the superluminal bound are given as follows

$$\bar{s}^{\mathrm{Kerr}}_{\mathrm{ISCO}} \approx -1.3200M, \qquad r^{\mathrm{Kerr}}_{\mathrm{ISCO}} \approx 3.5890M,$$
$$\bar{e}^{\mathrm{Kerr}}_{\mathrm{ISCO}} \approx 0.9237, \qquad \bar{l}^{\mathrm{Kerr}}_{\mathrm{ISCO}} \approx -3.0712M. \tag{45}$$

We have shown that the spinning test particle can orbit with more smaller radius in the RN and Kerr black hole backgrounds than the case in Schwarzschild black hole with the same mass M. The numerical results of the ISCO in the KN black hole background are also given in Fig. 10 and listed in Tables III, IV, V, VI, VII, VIII, and IX. Comparing the orbital frequency parameter in Tables VI and IX with the data in Tables I and II in Ref. [33] with the Tulczyew spin-supplementary condition, one can see that our results are exactly the same as that in Ref. [33].

We can make a brief summary that the change of parameters for the black hole and test particle can yield the following results:

(1) For the physical ISCO of the spinning test particle in the Schwarzschild black hole background, the corresponding radius and angular momentum decrease with the spin s, which indicates that the spinning test particle can orbit with more smaller radius than the nonspinning test particle with stable circular orbit.

(2) For the physical ISCO of the spinning test particle in the RN black hole background, the corresponding radius and angular momentum also decrease with the spin s, and this behavior is the same as the Schwarzschild case. In addition to the effect resulted from the spin s, the corresponding radius and

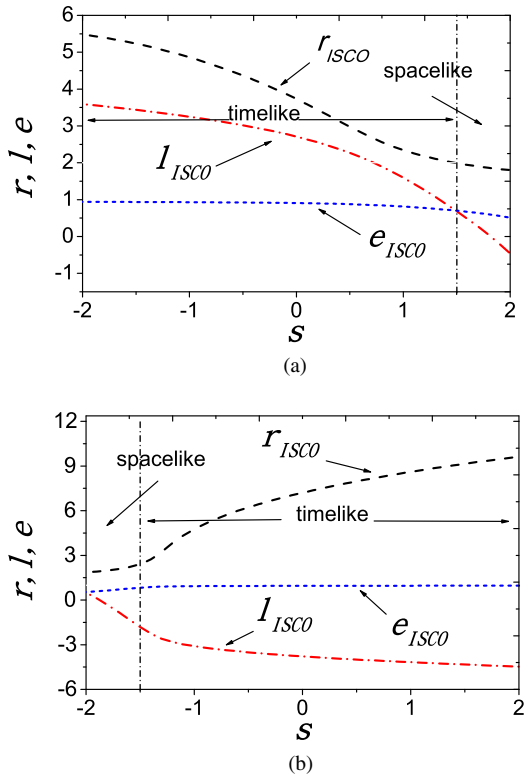

FIG. 10. Plots of the ISCO parameters of the spinning test particle with (a) corotating orbit and (b) counterrotating orbit as functions of the spin s in the KN black hole background. Only the left (right) side of the vertical line in upper (lower) figure stands for the timelike orbit. The parameters are set as $a/M = 0.5$, $Q/M = 0.5$.

angular momentum of the ISCO also decrease with the charge of the black hole Q, and the ISCO in the charged black hole is smaller than the Schwarzschild case with the same mass M.

(3) For the physical ISCO of the spinning test particle with corotating orbit in the nonextremal Kerr black hole background, the corresponding radius and angular momentum also decrease with the spin s, which is consistent with the Schwarzschild and RN cases. The corresponding radius and angular momentum of the ISCO also decrease with the spin of the black hole a. We should note that the radius of

TABLE III. The ISCO parameters of the spinning test particle in KN black hole background with charge $Q/M = 0$ and spin $a/M = 0$.

s	r_{ISCO}	l_{ISCO}	e_{ISCO}	$\Omega^{\frac{2}{3}}$
−0.9000	7.2135	3.8542	0.9528	0.1455
−0.7000	6.9807	3.7792	0.9512	0.1490
−0.5000	6.7294	3.6985	0.9492	0.1530
−0.3000	6.4568	3.6111	0.9470	0.1578
−0.1000	6.1594	3.5156	0.9443	0.1634
0.1000	5.8325	3.4097	0.9411	0.1702
0.3000	5.4700	3.2906	0.9371	0.1787
0.5000	5.0633	3.1533	0.9319	0.1894
0.7000	4.6028	2.9901	0.9248	0.2035
0.9000	4.0834	2.7871	0.9143	0.2224

TABLE IV. The ISCO parameters of the spinning test particle with corotating orbits in KN black hole background with charge $Q/M = 0.25$ and spin $a/M = 0.25$.

s	r_{ISCO}	l_{ISCO}	e_{ISCO}	$\Omega^{\frac{2}{3}}$
−0.9000	6.2035	3.5990	0.9454	0.1678
−0.7000	5.9854	3.5187	0.9432	0.1720
−0.5000	5.7480	3.4317	0.9406	0.1770
−0.3000	5.4888	3.3366	0.9376	0.1830
−0.1000	5.2049	3.2315	0.9340	0.1901
0.1000	4.8925	3.1136	0.9295	0.1989
0.3000	4.5478	2.9790	0.9237	0.2098
0.5000	4.1681	2.8214	0.9159	0.2237
0.7000	3.7575	2.6314	0.9051	0.2412
0.9000	3.3391	2.3954	0.8892	0.2627

TABLE V. The ISCO parameters of the spinning test particle with corotating orbits in KN black hole background with charge $Q/M = 0.5$ and spin $a/M = 0.5$.

s	r_{ISCO}	l_{ISCO}	e_{ISCO}	$\Omega^{\frac{2}{3}}$
−0.9000	4.7742	3.2074	0.9300	0.2133
−0.7000	4.5818	3.1169	0.9267	0.2189
−0.5000	4.3679	3.0173	0.9226	0.2257
−0.3000	4.1313	2.9062	0.9176	0.2342
−0.1000	3.8710	2.7809	0.9113	0.2446
0.1000	3.5877	2.6371	0.9032	0.2576
0.3000	3.2859	2.4691	0.8923	0.2734
0.5000	2.9790	2.2695	0.8775	0.2923
0.7000	2.6909	2.0308	0.8570	0.3132
0.9000	2.4462	1.7496	0.8296	0.3347

TABLE VI. The ISCO parameters of the spinning test particle with corotating orbits in KN black hole background with charge $Q/M = 0$ and spin $a/M = 0.9$.

s	r_{ISCO}	l_{ISCO}	e_{ISCO}	$\Omega^{\frac{2}{3}}$
−0.9000	3.1472	2.7401	0.8963	0.3138
−0.7000	3.0108	2.6334	0.8898	0.3197
−0.5000	2.8411	2.5102	0.8813	0.3294
−0.3000	2.6440	2.3665	0.8698	0.3430
−0.1000	2.4294	2.1965	0.8542	0.3605
0.1000	2.2155	1.9943	0.8327	0.3809
0.3000	2.0255	1.7559	0.8038	0.4023
0.5000	1.8727	1.4822	0.7666	0.4228
0.7000	1.7549	1.1762	0.7208	0.4420
0.9000	1.6634	0.8386	0.6653	0.4602

TABLE VII. The ISCO parameters of the spinning test particle with counterrotating orbits in KN black hole background with charge $Q/M = 0.25$ and spin $a/M = -0.25$.

s	r_{ISCO}	l_{ISCO}	e_{ISCO}	$\Omega^2_{\frac{s}{5}}$
−0.9000	7.9608	4.0285	0.9573	0.1321
−0.7000	7.7183	3.9566	0.9559	0.1351
−0.5000	7.4576	3.8797	0.9543	0.1386
−0.3000	7.1759	3.7968	0.9524	0.1426
−0.1000	6.8696	3.7068	0.9503	0.1474
0.1000	6.5335	3.6078	0.9477	0.1531
0.3000	6.1606	3.4974	0.9446	0.1601
0.5000	5.7404	3.3716	0.9406	0.1689
0.7000	5.2567	3.2240	0.9352	0.1806
0.9000	4.6851	3.0423	0.9275	0.1970

TABLE VIII. The ISCO parameters of the spinning test particle with counterrotating orbits in KN black hole background with charge $Q/M = 0.5$ and spin $a/M = -0.5$.

s	r_{ISCO}	l_{ISCO}	e_{ISCO}	$\Omega^2_{\frac{s}{5}}$
−0.9000	8.4901	4.1412	0.9601	0.1235
−0.7000	8.2408	4.0712	0.9588	0.1262
−0.5000	7.9734	3.9965	0.9574	0.1293
−0.3000	7.6852	3.9163	0.9558	0.1329
−0.1000	7.3724	3.8295	0.9540	0.1371
0.1000	7.0296	3.7345	0.9518	0.1422
0.3000	6.6494	3.6292	0.9491	0.1483
0.5000	6.2201	3.5101	0.9457	0.1560
0.7000	5.7223	3.3714	0.9413	0.1662
0.9000	5.1201	3.2023	0.9350	0.1807

TABLE IX. The ISCO parameters of the spinning test particle with counterrotating orbits in KN black hole background with charge $Q/M = 0$ and spin $a/M = -0.9$.

s	r_{ISCO}	l_{ISCO}	e_{ISCO}	$\Omega^2_{\frac{s}{5}}$
−0.9000	10.0629	4.4944	0.9661	0.1052
−0.7000	9.7986	4.4296	0.9652	0.1073
−0.5000	9.5171	4.3610	0.9642	0.1098
−0.3000	9.2155	4.2879	0.9630	0.1125
−0.1000	8.8903	4.2095	0.9617	0.1157
0.1000	8.5365	4.1248	0.9602	0.1194
0.3000	8.1468	4.0322	0.9584	0.1238
0.5000	7.7104	3.9294	0.9562	0.1293
0.7000	7.2088	3.8128	0.9535	0.1363
0.9000	6.6062	3.6759	0.9498	0.1459

the ISCO in the extremal Kerr black hole background with co-rotating orbit approach to the horizon r_h. And the ISCO radius and frequency is independent of the spin of test particle. For the ISCO with counterrotating orbit in the nonextremal Kerr black hole background, the radius of the ISCO decreases with the black hole spin a.

(4) For the physical ISCO of the spinning test particle in the KN hole background, the corresponding radius and angular momentum also decrease with the spin s. We have shown that the radius of the ISCO will decrease with the spin a and charge Q of the black hole. The most smallest radius of the ISCO in the KN black always appears in the case of the extremal KN black hole with spin $a = M$ (extremal Kerr black hole).

IV. SUMMARY AND CONCLUSION

In this paper, we have numerically investigated the ISCO of a spinning test particle in the Schwarzschild black hole, RN black hole, Kerr black hole, and KN black hole backgrounds. We used Eqs. (5) and (6) to describe the motion of the spinning test particle in curved spacetime, while the four-velocity of the spinning test particle can be transformed from timelike into spacelike due to the four-velocity vector u^μ and the conjugate momentum P^μ are not parallel. We gave the superluminal constraint (41) for the physical ISCO of the spinning test particle in various black hole backgrounds. We numerically gave the relations between the ISCO parameters and the spin s and showed that a spinning test particle can orbit in more smaller circular orbit than a nonspinning test particle. The radius of the ISCO for a spinning test particle was also affected by the charge and spin of the black hole, and the radius of the ISCO in the RN and Kerr black hole backgrounds are smaller than the case in Schwarzschild black hole. Although the radius of the ISCO decreases with the spin of the test particle s, we should note that the radius of the ISCO with corotating orbit in an extremal Kerr black can not decrease any more because of the corresponding radius is the horizon of the extremal Kerr black hole. We should note that the ISCO parameters depend on the spin-supplementary conditions and the pole-dipole approximation.

ACKNOWLEDGMENTS

We thank the referee for pointing out that the worldline of the spinning test particle depends on the choice of the spin-supplementary conditions and for his/her suggestions which led to the improvement of this paper. This work was supported in part by the National Natural Science Foundation of China (Grants No. 11522541, No. 11375075, No. 11675064, and No. 11205074), and the Fundamental Research Funds for the Central Universities (Grants Nos. lzujbky-2016-115 and No. lzujbky-2017-it68).

[1] S. A. Kaplan, J. Exp. Theor. Phys. **19**, 951 (1949).
[2] For more detailed description, see the book [64].
[3] B. P. Abbott *et al.* (LIGO Scientific Collaboration and Virgo Collaboration), Phys. Rev. Lett. **116**, 061102 (2016).
[4] B. P. Abbott *et al.* (LIGO Scientific Collaboration and Virgo Collaboration), Phys. Rev. Lett. **116**, 241103 (2016).
[5] B. P. Abbott *et al.* (LIGO Scientific Collaboration and Virgo Collaboration), Phys. Rev. Lett. **118**, 221101 (2017).
[6] B. P. Abbott *et al.* (LIGO Scientific Collaboration and Virgo Collaboration), Phys. Rev. Lett. **119**, 141101 (2017).
[7] B. P. Abbott *et al.* (LIGO Scientific Collaboration and Virgo Collaboration), Phys. Rev. Lett. **119**, 161101 (2017).
[8] http://lisa.jpl.nasa.gov.
[9] J. Luo *et al.*, Classical Quantum Gravity **33**, 035010 (2016).
[10] S. Suzuki and K. Maeda, Phys. Rev. D **58**, 023005 (1998).
[11] M. Shibata, K. Taniguchi, and T. Nakamura, Prog. Theor. Phys. Suppl. **128**, 295 (1997).
[12] J. L. Zdunik, P. Haensel, D. Gondek-Rosinska, and E. Gourgoulhon, Astron. Astrophys. **372**, 535 (2001).
[13] T. W. Baumgarte, AIP Conf. Proc. **575**, 176 (2001).
[14] P. Grandclement, E. Gourgoulhon, and S. Bonazzola, Phys. Rev. D **65**, 044021 (2002).
[15] M. A. Miller, P. Gressman, and W.-M. Suen, Phys. Rev. D **69**, 064026 (2004).
[16] P. Marronetti, M. D. Duez, S. L. Shapiro, and T. W. Baumgarte, Phys. Rev. Lett. **92**, 141101 (2004).
[17] D. Gondek-Rosinska, M. Bejger, T. Bulik, E. Gourgoulhon, P. Haensel, F. Limousin, and L. Zdunik, Adv. Space Res. **39**, 271 (2007).
[18] M. Campanelli, C. O. Lousto, and Y. Zlochower, Phys. Rev. D **73**, 061501 (2006).
[19] P. Shahrear and S. B. Faruque, Int. J. Mod. Phys. D **16**, 1863 (2007).
[20] C. Cabanac, R. P. Fender, R. J. H. Dunn, and E. G. Koerding, Mon. Not. R. Astron. Soc. **396**, 1415 (2009).
[21] A. Abdujabbarov and B. Ahmedov, Phys. Rev. D **81**, 044022 (2010).
[22] S. Hadar, B. Kol, E. Berti, and V. Cardoso, Phys. Rev. D **84**, 047501 (2011).
[23] S. Akcay, L. Barack, T. Damour, and N. Sago, Phys. Rev. D **86**, 104041 (2012).
[24] S. Hod, Phys. Rev. D **87**, 024036 (2013).
[25] C. Chakraborty, Eur. Phys. J. C **74** (2014), 2759.
[26] S. Hod, Eur. Phys. J. C **74**, 2840 (2014).
[27] O. B. Zaslavskii, Eur. Phys. J. C **75**, 403 (2015).
[28] S. Isoyama, L. Barack, S. R. Dolan, A. Le Tiec, H. Nakano, A. G. Shah, T. Tanaka, and N. Warburton, Phys. Rev. Lett. **113**, 161101 (2014).
[29] A. M. Al Zahrani, Phys. Rev. D **90**, 044012 (2014).
[30] T. Delsate, J. V. Rocha, and R. Santarelli, Phys. Rev. D **92**, 084028 (2015).
[31] G. Chartas, H. Krawczynski, L. Zalesky, C. S. Kochanek, X. Dai, C. W. Morgan, and A. Mosquera, Astrophys. J. **837**, 26 (2017).
[32] E. Harms, G. Lukes-Gerakopoulos, S. Bernuzzi, and A. Nagar, Phys. Rev. D **94**, 104010 (2016).
[33] G. Lukes-Gerakopoulos, E. Harms, S. Bernuzzi, and A. Nagar, Phys. Rev. D **96**, 064051 (2017).
[34] P. Jai-akson, A. Chatrabhuti, O. Evnin, and L. Lehner, Phys. Rev. D **96**, 044031 (2017).
[35] F. Chaverri-Miranda, F. Frutos-Alfaro, P. Gomez-Ovarez, and A. Oliva-Mercado, arXiv:1707.08663.
[36] N. Warburton and L. Barack, Phys. Rev. D **83**, 124038 (2011).
[37] M. van de Meent, Phys. Rev. Lett. **118**, 011101 (2017).
[38] A. J. Hanson and T. Regge, Ann. Phys. (N.Y.) **87**, 498 (1974).
[39] Robert M. Wald, Phys. Rev. D **6**, 406 (1972).
[40] P. I. Jefremov, O. Yu. Tsupko, and G. S. Bisnovatyi-Kogan, Phys. Rev. D **91**, 124030 (2015).
[41] M. Mathisson, Acta Phys. Pol. **6**, 163 (1937).
[42] A. Papapetrou, Proc. R. Soc. A **209**, 248 (1951).
[43] E. Corinaldesi and A. Papapetrou, Proc. R. Soc. A **209**, 259 (1951).
[44] W. G. Dixon, Proc. R. Soc. A **314**, 499 (1970).
[45] S. A. Hojman, Ph.D. thesis, Princeton University, 1975.
[46] R. Hojman and S. Hojman, Phys. Rev. D **15**, 2724 (1977).
[47] N. Zalaquett, S. A. Hojman, and F. A. Asenjo, Classical Quantum Gravity **31**, 085011 (2014).
[48] R. Uchupol, J. V. Sarah, and A. H. Scott, Phys. Rev. D **94**, 044008 (2016).
[49] C. Armaza, M. Banados, and B. Koch, Classical Quantum Gravity **33**, 105014 (2016).
[50] S. A. Hojman and F. A. Asenjo, Classical Quantum Gravity **30**, 025008 (2013).
[51] A. A. Deriglazov and W. G. Ramírez, Int. J. Mod. Phys. D **26**, 1750047 (2017).
[52] A. A. Deriglazov and W. G. Ramírez, Adv. High Energy Phys. **2016**, 1 (2016).
[53] W. G. Ramírez and A. A. Deriglazov, Phys. Rev. D **96**, 124013 (2017).
[54] A. A. Deriglazov and W. G. Ramírez, Adv. Theor. Math. Phys. **2017**, 7397159 (2017).
[55] J. Steinhoff and D. Puetzfeld, Phys. Rev. D **81**, 044019 (2010).
[56] W.-B. Han, Gen. Relativ. Gravit. **40**, 1831 (2008); **49**, 48 (2017).
[57] W.-B. Han, Phys. Rev. D **82**, 084013 (2010).
[58] N. Warburton, T. Osburn, and C. R. Evans, Phys. Rev. D **96**, 084057 (2017).
[59] G. Faye, L. Blanchet, and A. Buonanno, Phys. Rev. D **74**, 104033 (2006).
[60] G. Lukes-Gerakopoulos, J. Seyrich, and D. Kunst, Phys. Rev. D **90**, 104019 (2014).
[61] L. Filipe Costa, G. Lukes-Gerakopoulos, and O. Semerák, arXiv:1712.07281.
[62] G. Lukes-Gerakopoulos, E. Harms, S. Bernuzzi, and A. Nagar, Phys. Rev. D **96**, 064051 (2017).
[63] Y.-P. Zhang, B.-M. Gu, S.-W. Wei, J. Yang, and Y.-X. Liu, Phys. Rev. D **94**, 124017 (2016).
[64] L. D. Landau and E. M. Lifshitz, *The Classical Theory of Fields* (Pergamon, Oxford, 1993).
[65] J. M. Bardeen, W. H. Press, and S. A Teukolsky, Astrophys. J. **178**, 347 (1972).